

Polarization rotation and exact transverse electromagnetic wave solutions in topological insulatorsSebastián Filipini¹* and Mauro Cambiaso¹†*Departamento de Ciencias Físicas, Facultad de Ciencias Exactas, Universidad Andres Bello, Avenida República 220, Santiago, Chile*

(Received 3 August 2023; revised 24 February 2024; accepted 7 May 2024; published 3 June 2024)

In the context of θ electrodynamics we find transverse electromagnetic wave solutions forbidden in Maxwell electrodynamics. Our results attest to different signatures of the topological magnetoelectric effect in topological insulators, resulting from a polarization rotation of an external electromagnetic field. Unlike Faraday and Kerr rotations, the effect does not rely on a longitudinal magnetic field, the reflected field, or birefringence. The rotation occurs due to transversal discontinuities of the topological magnetoelectric parameter in cylindrical geometries. The dispersion relation is linear, and birefringence is absent. Exact transversality allows electromagnetic waves to propagate in an optical fiber without successive total internal reflections, diminishing losses, and regardless of acute bends of the fiber. These results may open other possibilities in optics and photonics by utilizing topological insulators to manipulate light.

DOI: [10.1103/PhysRevB.109.235108](https://doi.org/10.1103/PhysRevB.109.235108)**I. INTRODUCTION**

The topological magnetoelectric effect (TME) has been intensely sought after in recent decades as a definitive signal of quantum states of matter possessing topological order [1–9]. Topological insulators (TIs) are among the most well-known and studied cases presenting TME. These new quantum states can be found in heterostructures of elements such as Bi, Se, Te, Sb, and others [10–14]. They exhibit conducting edge/surface states protected against disorder by time-reversal symmetry, with properties differing from those in the bulk of the material, which is gapped as conventional insulators [15,16].

Due to their microscopic structure, three-dimensional (3D) TIs have unique electromagnetic (EM) responses that can be described macroscopically by the axionic θ term $\mathcal{L}_\theta = (\theta/4\pi)\mathbf{E} \cdot \mathbf{B}$ [17]. In the context of TIs, $\theta = \frac{\alpha}{\pi}\theta_{\text{TI}}$, where α is the fine-structure constant and θ_{TI} is called the topological magnetoelectric polarizability (TMEP). Its origin is quantum mechanical and it encodes the microscopic properties that characterize TIs. This provides a correct description of the system if an appropriate time-reversal symmetry breaking perturbation is introduced to gap the surface states, which results in the material (in its bulk and at the surface) becoming an insulator. The surface, however, is a quantum Hall insulator rather than a normal one. The latter can be achieved by adding a magnetic perturbation (applied field and/or film coating) [18,19], or by using commensurate out-of-plane and in-plane antiferromagnetic or ferrimagnetic insulating thin films [20]. As a result, θ_{TI} becomes quantized in odd-integer values of π , i.e., $\theta_{\text{TI}} = \pm(2n + 1)\pi$, where $n \in \mathbb{Z}$ and the sign is determined by the time-reversal symmetry breaking perturbation. This gives a valid description of the EM response of TI provided $\hbar\omega \ll E_g$, with ω the frequency of the EM field and E_g the surface gap. Trivial insulators have $\theta_{\text{TI}} = 0$. In this paper,

θ_{TI} will be taken as a constant parameter characteristic of each medium. For brevity we will simply write θ and we shall refer to this theory as θ -electrodynamics (θ -ED) rather than axion electrodynamics. This model can also describe Tellegen magnetoelectric media [21–24] and Weyl semimetals when $\theta(\mathbf{x}, t) = 2(\mathbf{b} \cdot \mathbf{x} - b_0 t)$, where \mathbf{b} is the separation in momentum space between the Weyl nodes and b_0 their separation in energy [25,26]. Magnetoelectric responses due to chirality have been considered in Ref. [27], however, these are not equivalent to the ones considered here [28,29]. In this paper, we will focus on TME signals stemming from the EM response of TIs following closely the methodology of Refs. [30–32] and also similar to what has been done, for example, to study Faraday rotation [33–37], induced magnetic-monopole-like fields [38], and topologically induced effects in cavities and slab waveguides [39,40]. On the other hand, whenever a no-go theorem can be circumvented, a door into new theoretical and/or experimental possibilities is opened. In Ref. [31] it was shown that θ -boundary value problems can evade Earnshaw's theorem, which implies that transverse EM (TEM) fields cannot propagate in media with less than two conductors. Hence, as one of the most striking effects of θ -ED is to modify the boundary conditions (BCs) that the fields must satisfy, in this paper we pursue this idea in systems that are heavily reliant on BCs to find TEM wave solutions that are possible due to the magnetoelectricity of Tellegen materials, of which TIs are a particular kind, thus providing observable signatures of the elusive TME that are different from those previously reported in the literature. Our findings pave the way to other means of harnessing light with possible applications in photonics that are yet to be discovered.

The paper is organized as follows. In Sec. II we review the basics of θ -electrodynamics. That is to say the field equations for Maxwell's Lagrangian appended with the axion term commented above, emphasizing how the θ term modifies the boundary conditions that the fields must satisfy at spatial surfaces where θ is discontinuous. The field equations are decomposed in longitudinal and transverse components as is

*s.filipiniparra@uandresbello.edu

†mcambiaso@unab.cl

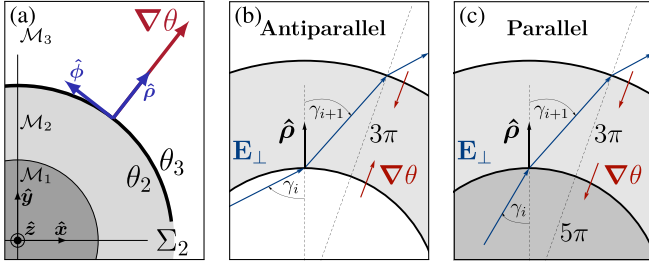


FIG. 1. In (a) we show a generic cylindrical geometry. Only three media \mathcal{M}_i are shown (each characterized by ϵ_i , μ_i , θ_i). In this example $\theta_1 = 0$, so Σ_2 , located at R_2 is the only θ interface and $\nabla\theta = (\theta_3 - \theta_2)\delta(\rho - R_2)\hat{\rho}$. In (b) and (c) different $\nabla\theta$ configurations are shown in which an EM wave propagates in the \hat{z} direction. (b) Antiparallel and (c) parallel refer to the directions of $\nabla\theta$ (red). The transverse \mathbf{E}_\perp fields are shown in blue.

customary for the study of field propagation in waveguides and/or optical fibers. In Sec. III we present the properties of the TEM fields, namely, the relation defining the transversality condition and the general dispersion relation. In this section we also introduce a rotation of the plane of polarization of the EM field propagating transversely to $\nabla\theta$ that is different to Faraday or Kerr rotations. In Sec. IV we present explicit solutions for the TEM fields inside and outside a single cylindrical TI with constant θ , impinged upon by an external background EM field that serves as an asymptotic boundary condition and comment on the role that different polarizations of the background EM field would have on the rotating effect of the TI and on the resulting spatial distribution of the EM field. Sec. V introduces the idea of considering several θ interfaces and the possibilities in terms of the possible configurations depending on the $\nabla\theta$ at each surface. More specifically, in Sec. V A we analyze the case of two θ interfaces. This divides the whole space in three cylindrical regions (a) $(0, R_1)$; (b) (R_1, R_2) ; and (c) (R_2, ∞) . For the TMEP of each region we will choose them in the ‘‘antiparallel’’ configuration as in Fig. 1(b). That is when the gradient of θ at both layers (and in the same angular direction) are antiparallel, and to simplify the analysis, we will furthermore choose the inner and outer regions as topologically trivial, such that the geometry is basically that of a cylindrical TI shell of finite width. In Sec. V B we analyze the power transmitted in the different cylindrical regions defined by the θ interfaces and compare it with the power that would be transmitted through the same regions but without the TI. In Sec. V C we elaborate criteria that allow us to speak of the confining capacity of the cylindrical TI shell on exact TEM fields that propagate in the TI, acting as an optical fiber. Finally, in Sec. VI we summarize our results, provide some context for the relevance of finding TEM solutions, and elaborate on possible extensions and applications of these ideas.

Throughout the paper, the equations of θ -ED will be written in Gaussian units. The coordinates (ρ, ϕ, z) are the cylindrical coordinates with z in the direction of the wave propagation and of the cylindrical surfaces. ρ and ϕ are the usual ones related to the Cartesian directions in Fig. 1(a), i.e., $\nabla\theta$ points in the radial direction $\hat{\rho}$, and $\hat{\phi}$ is perpendicular to the latter, in the anti-clockwise direction.

II. NONDYNAMICAL θ ELECTRODYNAMICS

In θ -ED, the source-free equations do not change, but Gauss and Ampère-Maxwell laws are

$$\nabla \cdot (\epsilon \mathbf{E}) = 4\pi \rho - \nabla\theta \cdot \mathbf{B}, \quad (1)$$

$$c \nabla \times (\mathbf{B}/\mu) - \partial_t(\epsilon \mathbf{E}) = 4\pi \mathbf{J} + c \nabla\theta \times \mathbf{E} + \dot{\theta} \mathbf{B}. \quad (2)$$

We will consider monochromatic harmonic EM fields, $\mathbf{E}(\mathbf{r}, t) = \mathbf{E}(\mathbf{r}_\perp)e^{i(kz - \omega t)}$ and similar for $\mathbf{B}(\mathbf{r}, t)$, propagating in cylindrical media with coaxial symmetry, and axis along \hat{z} as in Fig. 1(a). Coaxial cylindrical surfaces Σ separate each medium, such that $\nabla\theta = \tilde{\theta}_i \delta(\rho - R_i)\hat{\rho}$, where $\tilde{\theta}_i \equiv \theta_{i+1} - \theta_i$, θ_i being the value of the TMEP in the i th medium and R_i defines the interface Σ_i . TIs of cylindrical geometry have received considerable attention theoretically [32,40–43] and, despite possibly challenging, even experimentally [44]. We will consider all media with the same ϵ and μ . Decomposing vectors in directions longitudinal and transverse to the wave vector [45], the vacuum field equations that receive a θ -term modification read

$$\epsilon \nabla_\perp \cdot \mathbf{E}_\perp + [\tilde{\theta} B_\rho] = -ik\epsilon E_z, \quad (3)$$

$$ick\mathbf{B}_\perp - i\epsilon\mu\omega \hat{z} \times \mathbf{E}_\perp = c\nabla_\perp B_z - c\mu[\tilde{\theta} E_z \hat{\rho}], \quad (4)$$

$$c(\nabla_\perp \times \mathbf{B}_\perp)_z - c\mu[\tilde{\theta} E_\phi] = -i\epsilon\mu\omega E_z, \quad (5)$$

where $\partial_z\theta$ and $\dot{\theta}$ terms vanish. Given $\nabla\theta$ has support at the radial interfaces only, we have put e.g., $\nabla\theta \cdot \mathbf{B}_\perp = [\tilde{\theta} B_\rho]$.

III. TEM WAVE SOLUTIONS AND POLARIZATION ROTATION AS A TOPOLOGICAL MAGNETOELECTRIC SIGNATURE

Due to the $[\tilde{\theta} B_\rho]$ and $[\tilde{\theta} E_\phi]$ terms, the equations of θ -ED [i.e., Eqs. (3)–(5) together with those that do not acquire θ modifications] admit nontrivial TEM wave solutions for the EM fields, i.e., $\mathbf{E}_\perp \neq \mathbf{0}$, $\mathbf{B}_\perp = \sqrt{\epsilon\mu} \hat{z} \times \mathbf{E}_\perp$, and $E_z = 0 = B_z$, provided $ck = \omega \sqrt{\mu\epsilon}$ and $\sqrt{\epsilon_{i+1}\mu_{i+1}} = \sqrt{\epsilon_i\mu_i}$, where i and $i+1$ represent adjacent media. With this choice of θ , the fields propagate with a continuous wave number and without birefringence, as free TEM waves in an (ϵ, μ, θ) medium. Henceforth we will drop the subscript \perp and assume all media as nonmagnetic, so $\mu = 1$ for all media, thus $\epsilon_{i+1} = \epsilon_i = \epsilon$. The $\nabla\theta$ interface produces a discontinuity of \mathbf{E} that results in a rotation of the polarization of the field. This situation is depicted in Figs. 1(b) and 1(c). At any given point of the θ interface, the directions of the \mathbf{E} satisfy

$$\tan \gamma_{i+1} = \tan \gamma_i (1 + 2Z_\theta \tan \gamma_i)^{-1}, \quad (6)$$

where $Z = \sqrt{\mu/\epsilon}$ is the impedance, $Z_\theta \equiv \tilde{\theta}Z/2$, and γ_i, γ_{i+1} are the angles between the normal to the i th interface and \mathbf{E} on either side of it. This rotation is an interesting signature of the TME that differs radically from Faraday and Kerr rotation effects, which have also been predicted in the context of TIs as signals of the TME [33,36,37,46–51]. The rotation found here is not caused by a component of \mathbf{B} along the direction of propagation, neither is it due to birefringence, nor is it a property of the reflected field. This prediction leads to another way to observe the TME, and it is a consequence of exact

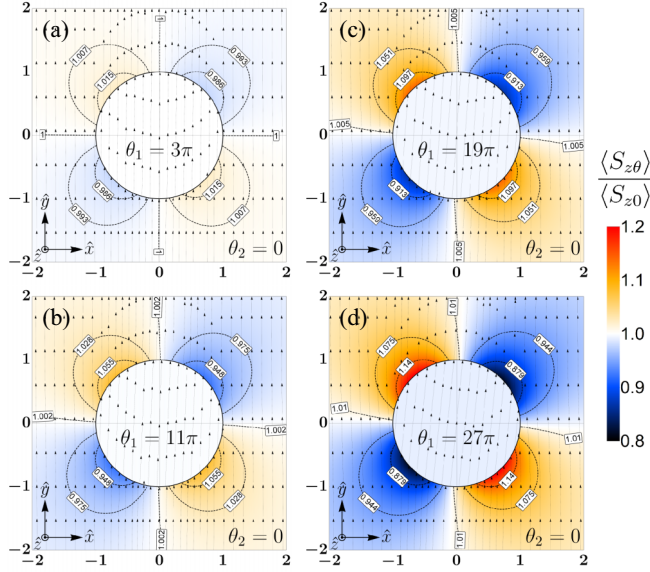


FIG. 2. Density plots of the relative Poynting vector in the interior and exterior regions relative to that of the background EM field. The streamlines are the total \mathbf{E} -field lines. The contour plots show contours of constant relative Poynting vector. (a)–(d) correspond to $Z = 1$ and $\theta = 3\pi, 11\pi, 19\pi, 27\pi$, respectively.

TEM wave solutions that had not been possible up until now and are certainly very vehemently sought after [52–56]. With several layers the cumulative effect is different for the parallel and antiparallel configurations of Figs. 1(b) and 1(c), because the effect is sensitive to $\tilde{\theta}$.

IV. ONE CYLINDRICAL θ INTERFACE IN AN EXTERNAL MONOCHROMATIC PLANE WAVE

Consider an infinitely long TI cylinder of radius R , characterized by θ in a homogeneous medium, both with the same Z . We seek solutions that asymptotically away from the TI tend to a plane wave with linear polarization (LP), say, in the \hat{y} direction, i.e., $\lim_{\rho \rightarrow \infty} \mathbf{E}(\rho, \phi, z, t) = E_0 e^{i(kz - \omega t)} \hat{y}$. The TEM fields that solve the θ -ED equations in each media \mathcal{M}_i , for $i = 1, 2$, are $\mathbf{E}_i = E_0 \hat{y} + E_0 \mathbf{E}_i^\theta$, where

$$\mathbf{E}_1^\theta = -\kappa(\hat{x} + Z_\theta \hat{y}), \quad (7)$$

$$\mathbf{E}_2^\theta = \kappa \ell^2 [(Z_\theta \sin \phi + \cos \phi) \hat{\rho} + (\sin \phi - Z_\theta \cos \phi) \hat{\phi}], \quad (8)$$

where $\kappa = Z_\theta / (1 + Z_\theta^2)$ and $\ell = R/\rho$. Since \mathbf{B} is determined by \mathbf{E} , henceforth we will mostly refer to \mathbf{E} . If $\tilde{\theta} = 0$ there is no interface and the interior and exterior solutions are identical to $E_0 e^{i(kz - \omega t)} \hat{y}$. If $E_0 = 0$, there is no solution at all, so our solution is reliant on the background field. But, if $\tilde{\theta} \neq 0$ and $E_0 \neq 0$, a total TEM solution exists in all space that cannot be obtained with all-dielectric materials or otherwise, and it acquires different and nontrivial features that are attributable to θ alone leading to other observable signatures of the TME.

A. Polarization rotation and field spatial distribution

Figure 2 shows \mathbf{E} -field streamlines, the spatial distribution, and the contour plots of the temporal average of the Poynt-

ing vector (relative to that of the background field: $\langle S_{z0} \rangle = cE_0^2/8\pi Z$). Inside the TI, \mathbf{E} is uniform, and, due to Eq. (6), the polarization rotates by a fixed amount. This rotation is given by

$$\cos \varphi_{\text{int}} = \hat{\mathbf{E}}_1 \cdot \hat{\mathbf{y}} = (1 + Z_\theta^2)^{-1/2}. \quad (9)$$

For $Z = 1$ and $\theta_{\text{TI}} = 3\pi, 11\pi, 19\pi$, and 27π , respectively, this implies a rotation of the polarization plane of $0.63^\circ, 2.30^\circ, 3.97^\circ$, and 5.63° , respectively, that is entirely due to the TMEP of the TI, differs from Faraday or Kerr rotations, and is within present-day experimental sensitivity.

The relative Poynting vectors $\mathcal{S}_z^\theta(\rho, \phi) \equiv \langle S_{z\theta} \rangle / \langle S_{z0} \rangle$ in each region are given by

$$\mathcal{S}_{z1}^\theta = 1 - \kappa Z_\theta, \quad (10)$$

$$\mathcal{S}_{z2}^\theta = 1 + \kappa [Z_\theta \ell^4 + 2\ell^2 (\sin 2\phi - Z_\theta \cos 2\phi)]. \quad (11)$$

Away from the TI's surface, the power per unit area varies as an anisotropic term that goes as ρ^{-2} , and by an isotropic term that goes as ρ^{-4} . We observe that $\mathcal{S}_z^\theta(\rho, \phi) = \mathcal{S}_z^\theta(\rho, \phi + n\pi)$ for $n = 1, 2, \dots$ and also $\mathcal{S}_z^\theta(\rho, \phi) - \mathcal{S}_z^\theta(\rho, -\phi) = 4\kappa \ell^2 \sin 2\phi = \mathcal{S}_z^\theta(\rho, \phi) - \mathcal{S}_z^\theta(\rho, \pi - \phi)$. Also, the relative Poynting, as a function of ϕ , has maxima and minima defined by the directions $\phi_\pm = \arctan(Z_\theta \pm \sqrt{1 + Z_\theta^2})$, respectively, corresponding to the lines (not drawn) in Fig. 2 of extremal intensities. In fact, $|\mathcal{S}_z^\theta(R, \phi_+) - 1| > |\mathcal{S}_z^\theta(R, \phi_-) - 1|$, however, with respect to the extremal directions, the relative Poynting is indeed symmetric, namely, $\mathcal{S}_z^\theta(\rho, \phi_\pm + \alpha) = \mathcal{S}_z^\theta(\rho, \phi_\pm - \alpha)$. This asymmetric field distribution can be understood self-consistently, order-by-order in θ , in terms of the induced topological surface charge densities. The jump in θ across the boundary times the \mathbf{B} -field normal to the cylinder generates a discontinuity of the \mathbf{E} -field that acts as a topological surface charge density $\sigma_\theta(\Sigma) = -\frac{1}{4\pi}(\tilde{\theta} \mathbf{B} \cdot \hat{\rho})|_\Sigma$. Along with it, there is an induced (topological) surface current density $\mathbf{K}_\theta(\Sigma) = \frac{c}{4\pi}(\tilde{\theta} \hat{\rho} \times \mathbf{E})|_\Sigma$ [57]. The total electric field $\mathbf{E}_{1,2}^\theta$ (and the corresponding $\mathbf{B}_{1,2}^\theta$) can be understood as an infinite superposition of the fields induced by these topological surface charge densities and currents. The infinite sum, in fact converges and lead precisely to the fields in Eqs. (7)–(8). Further details in [58].

B. The role of the polarization of the background field

If the background field has right-handed or left-handed circular polarizations (RCP/LCP), the amount of the polarization rotation inside the TI is the same and in each case it rotates in the same sense the background field does. At a given time and for appropriate initial conditions (or phase) the structure for the CP background field and the patterns of the Poynting vector are the same as for the LP. The temporal averages differ considerably, though. For the CP background field, the pattern of the external Poynting is isotropic only with a $\sim \tilde{\theta}^2 \rho^{-4}$ dependence [59].

To understand this, we realize that the Poynting has an interaction term $2E_0 \hat{y} \cdot E_0 \mathbf{E}^{\theta*}$ in either regions interior and exterior to the TI. Going back to our discussion of the induced topological polarization charges, for a CP background field, these σ_θ will also tend to redistribute following the direction

of the \mathbf{E} field, which is rotating itself so there is no misalignment between the background field and that produced by the induced charges, thus they remain orthogonal to each other at all times.

V. SEVERAL COAXIAL CYLINDRICAL θ INTERFACES IN AN EXTERNAL MONOCHROMATIC PLANE WAVE

The precise form of the repeated effects with several coaxial cylindrical θ interfaces depend on the different radii at which the θ interfaces lie, on $\nabla\theta$ at each layer and possibly on the polarization of the background EM field. With respect to the directions of $\nabla\theta$ there are several possible configurations. We will focus on the antiparallel configuration depicted in Fig. 1(b). The study of more θ -interfaces is left for elsewhere [58]. For simplicity we analyze the case of two θ interfaces.

A. Two coaxial θ interfaces in antiparallel configuration

Consider two θ interfaces in antiparallel configuration as depicted in Fig. 1(b), with the same background EM field as above. The geometry is as in Fig. 1(a), with $\theta = \theta_2 \neq 0$ for $R_1 \leq \rho < R_2$ and zero elsewhere. In regions $i = 1, 2, 3$ the total electric field is indeed TEM, can be written as $\mathbf{E}_i = E_0\hat{\mathbf{y}} + E_0\Theta_\chi\mathbf{E}_i^\theta$, and the θ contributions are

$$\mathbf{E}_1^\theta = -Y\theta_2\hat{\mathbf{y}}, \quad (12)$$

$$\mathbf{E}_2^\theta = \left[2\frac{R_1^2}{\rho^2}(\cos\phi\hat{\rho} + \sin\phi\hat{\phi}) + 2\hat{\mathbf{x}} - Y\theta_2\hat{\mathbf{y}} \right], \quad (13)$$

$$\mathbf{E}_3^\theta = \frac{YR_2^2}{\rho^2} \left[\sin\phi \left(\theta_2\hat{\rho} - \frac{2\hat{\phi}}{Z} \right) - \cos\phi \left(\frac{2\hat{\rho}}{Z} + \theta_2\hat{\phi} \right) \right], \quad (14)$$

where $\chi = R_1/R_2$, $Y = Z(1 - \chi^2)$, and $\Theta_\chi = Z\theta_2/(4 + YZ\theta_2^2)$. Despite the value of θ_2 , the field in region 1 is uniform, with the same polarization as the asymptotic background field and χ determines how much is the intensity diminished in there. In Figs. 3(a) and 3(b) we show the density plots of the temporal average of the Poynting vector relative to the background, and \mathbf{E} -field streamlines, corresponding to Eqs. (12)–(14), for $Z = 1$ and $\theta_2 = 27\pi$. In Fig. 3(a), $\chi_a = 0.45$, and in Fig. 3(b), $\chi_b = 0.82$, respectively. For smaller θ the same effects arise, but fainter. In either case, in the TI's bulk the field is similar in its asymmetric quadrupolarlike distribution, as for one θ layer, but it is inverted with respect to the exterior region.

B. Transmitted power in each region, as a function of θ and the geometry of the system

In Fig. 3(c), for different values of θ , we compare the power transmitted in region 1,

$$P_1^{\theta_2}(\chi) = \int_0^{R_1} \langle S_{z\theta} \rangle ds_\perp, \quad (15)$$

to the power transmitted in that same region by the background field, $P_1^{\theta_2=0}$ (in solid black line). For fixed χ , we see that $P_1^{\theta_2}$ is smaller for higher values of θ and, for a given θ , $P_1^{\theta_2}$ scales with R_1 (which is rather trivial as the bigger/smaller R_1 , the bigger/smaller the area pierced by the Poynting). The

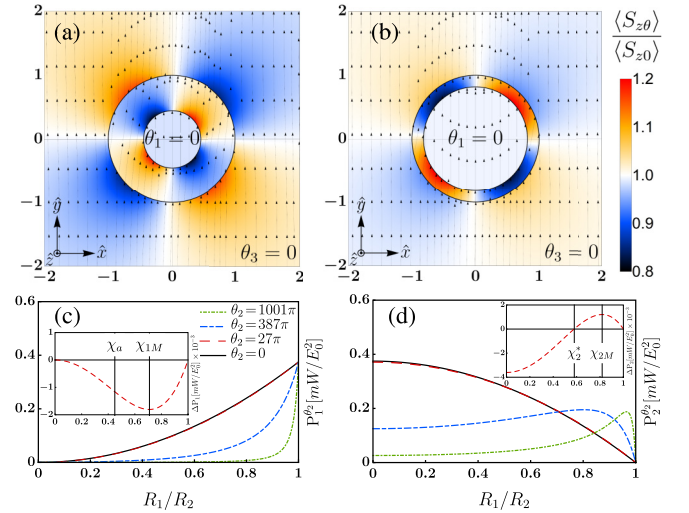


FIG. 3. In all cases $Z = 1$. In (a), (b) $\theta_1 = 0 = \theta_3$ and $\theta_2 = 27\pi$ inside the TI. In (a) $\chi = 0.45$ and in (b) $\chi = 0.82$. (c) and (d) show the power transmitted through regions 1 and 2, $P_1^{\theta_2}$ and $P_2^{\theta_2}$, respectively, for $R_2 = 10 \mu\text{m}$. For $\theta_2 = 0$, the corresponding powers, $P_{1,2}^{\theta_2=0}$, are shown in the solid black line. For $\theta_2 = 27\pi$, the inset of (c) shows ΔP_1 . The vertical lines are $\chi_a = 0.45$ which defines the geometry of the configuration in (a), and χ_{1M} that maximizes the difference. The inset of (d) shows ΔP_2 and the values χ_2^* and χ_{2M} .

differences $\Delta P_i(\chi) \equiv P_i^{\theta_2} - P_i^{\theta_2=0}$ for $i = 1, 2$ quantify how much of the θ contribution to the EM field is trapped or “confined” in region i . The quantities $P_2^{\theta_2}(\chi)$ correspond to the transmitted power by the EM field through the region $R_1 \leq \rho \leq R_2$ with TI (θ) and without (0), respectively, namely,

$$P_2^{\theta_2}(\chi) = \int_{R_1}^{R_2} \langle S_{z\theta} \rangle ds_\perp. \quad (16)$$

Their χ dependence allows to find optimal configurations, e.g., for any given θ_2 , there is a critical $\chi_{1M}(\theta_2)$ that minimizes ΔP_1 . The inset to Fig. 3(c) shows this difference and the values χ_a and $\chi_{1M}(27\pi)$. Rather surprisingly, in the $R_1 \rightarrow R_2$ limit, a radial and anisotropic electric field residing only at $\rho = R_2$ remains while in regions 1 and 3 the total electric field is exactly equal to the background field.

C. Geometry optimization and confinement of the TEM field inside the TI

Similarly, in Fig. 3(d), for different values of θ , we compare the power transmitted in region 2, $P_2^{\theta_2}(\chi)$, to that transmitted in the same region by the background field, $P_2^{\theta_2=0}$ (in the solid black line). For every given $\theta_2 \neq 0$, there exists a $\chi_2^*(\theta_2)$ such that $\Delta P_2(\chi_2^*) > 0$, i.e., for which the power transmitted in the TI's bulk exceeds that in the same region if the TI were absent. This occurs when the $\theta_2 \neq 0$ curves cross the solid black line ($\theta_2 = 0$). Regardless the value of θ_2 such an intersection always occurs, but it is more evident for larger values of θ_2 (compare the red (dashed) curve to the blue (dotted-dashed) or green (smaller dotted-dashed) curves). The bigger the θ_2 , the larger the gain, however, the closer χ must be to 1, i.e., higher yields occur for higher θ and through thinner TI sheaths. Furthermore, for that given θ_2 , there

exists a $\chi_{2M}(\theta_2)$ with $\chi_2^* < \chi_{2M} < 1$ that maximizes ΔP_2 . In Fig. 3(d), we chose $\chi = \chi_{2M}$ for which $P_2^{\theta_2=27\pi}(\chi_{2M}) = \max[P_2^{\theta_2=27\pi}(\chi)] = 1.01P_2^{\theta_2=0}(\chi_{2M})$.

A priori, one could have expected that for a given θ_2 that configuration that minimizes the power transmitted through region 1 (inner vacuum core) is the same configuration that maximizes the power transmitted through region 2 (inside the TI). Namely, the expectation that the power gain through the TI is at the expense of the loss of power in the inner vacuum core, as if the TI sucked power from the inner shells only. Rather surprisingly, this is not the case. In fact, for $\theta_1 = 0$ we can show that there is no χ that minimizes $P_1^{\theta_2}$ and simultaneously maximizes $P_2^{\theta_2}$, implying that both geometry optimization procedures described are in fact independent. To contrast the explanation above, the physical reason for this would then be that not only does the TI confine the EM field in its bulk by depleting the EM field in the inner vacuum, but does so with the field exterior to the TI too. This is why the density plot of the Poynting distribution, for a fixed angular direction and fixed external radius $R < \rho$, is fainter in Fig. 3(b) than it does in Fig. 3(a).

VI. SUMMARY AND CONCLUSIONS

As mentioned, in θ -ED, Earnshaw's theorem no longer applies [60], thus enlarging the space of solutions. In fact, due to the TMEP of the TI, here we find nontrivial TEM wave solutions confined inside the TI that are impossible in ordinary Maxwell theory. Hosting TEM waves in optical fibers is highly prized in optics and photonics. The exact TEM wave solutions have a linear dispersion relation, thus waves propagate without cutoff frequencies. Losses are reduced by having no conductors and because the EM waves propagate in an exact transverse manner. This contrasts TE or TM propagation, in which the field undergoes successive internal reflections suffering losses at each reflection and furthermore, the incident angle cannot exceed the critical one above which the EM field no longer reflects but rather gets refracted outside the fiber. This attribute is highly appealing for miniaturized devices, as it allows the TI-optical fiber to be bent in any angle.

In summary, we found exact TEM waves propagating along the axis of cylindrical media that are impossible except for Tellegen materials and, in particular, for TIs. The aforementioned surface charge and current densities are induced at the θ interfaces and oscillate in time such that the boundary conditions are satisfied at every instant of time. These TEM fields propagate both outside the cylindrical TIs as asymptotic free solutions and inside each of the geometries, with a lin-

ear dispersion relation as in a free medium, without cutoff frequencies and without birefringence. Finite discontinuities of the TMEP at the interface between each layer result in a rotation of the polarization plane of the EM field. This rotation is different from Faraday or Kerr rotations for TIs, attesting to a different observable signature of the TME. In the case of a single θ layer the field exhibits an asymmetric quadrupolar distribution in the plane perpendicular to the TI. Most TIs known have $\epsilon \neq 1$. Their dielectric function is typically described by an oscillatorlike model leading to material dispersion $\epsilon(\omega)$, with characteristic oscillator strengths, resonant frequency, and damping coefficient, usually negligible with respect to the latter (see, e.g., Ref. [61]). For TIBiSe₂ with $\theta_{\text{TI}} = 11\pi$ and $\epsilon = 4$ as reported in Ref. [62] and for Bi₂Se₃ with $\theta_{\text{TI}} = \pi$ and $\epsilon = 16$ as reported in Ref. [36], the rotations of the plane of polarization inside the cylindrical TI are 20.07 and 0.91 mrad, respectively. For the nontopological magnetoelectric TbPO₄, with $\theta = 0.22$ and $\epsilon = 3.5$ [63], the rotation would be of 58.7 mrad. For the case of two θ layers, the field propagates along the TI's bulk as in an optical fiber. Its confinement can be improved varying χ and θ , though ϵ must be the same for all media. TEM wave solutions are possible at the expense of not being able to vary the permittivities as is usually done to improve the confinement of the EM fields in all-dielectric and metamaterial waveguides. Our results point towards other directions for light manipulation purposes and for studying different manifestations of the TME. We have put $Z = \sqrt{\mu/\epsilon} = 1$, as in Ref. [35], to focus on the dependence on $\nabla\theta \neq \mathbf{0}$. As our predictions are proportional to $Z\tilde{\theta}$, real TIs with $1 < \epsilon$ (say, ~ 16) would diminish the effects, but increasing θ (say, from π to 5π) could compensate for this. Lastly, analytical solutions with several TI cylinders are cumbersome. Preliminary numerical calculations indicate that an *ad hoc* array of several parallel TI cylinders would result in a considerable gain of observable signatures of the TME, due to an enhancement of the Poynting vector by means of superposition. These and other open questions will be dealt with in Ref. [58].

ACKNOWLEDGMENTS

We thank L. F. Urrutia and A. Martín-Ruiz for useful comments and careful reading of the manuscript, and Instituto de Ciencias Nucleares at UNAM, for the hospitality during early stages of this work. Both authors acknowledge support from the project CONAHCYT CF/2019/428214. S.F. has been funded by Scholarship Program/BECAS DOCTORADO UNAB and M.C. has been funded by Universidad Andres Bello UNAB DI-16-20/REG internal project.

- [1] F. D. M. Haldane and L. Chen, *Phys. Rev. Lett.* **53**, 2591 (1984).
- [2] J. M. Kosterlitz and D. J. Thouless, *J. Phys. C: Solid State Phys.* **6**, 1181 (1973).
- [3] R. B. Laughlin, *Phys. Rev. B* **23**, 5632 (1981).
- [4] D. J. Thouless, M. Kohmoto, M. P. Nightingale, and M. den Nijs, *Phys. Rev. Lett.* **49**, 405 (1982).

- [5] C. L. Kane and E. J. Mele, *Phys. Rev. Lett.* **95**, 146802 (2005).
- [6] B. A. Bernevig, T. L. Hughes, and S.-C. Zhang, *Science* **314**, 1757 (2006).
- [7] J. E. Moore and L. Balents, *Phys. Rev. B* **75**, 121306(R) (2007).
- [8] L. Fu, C. L. Kane, and E. J. Mele, *Phys. Rev. Lett.* **98**, 106803 (2007).

- [9] L. Fu and C. L. Kane, *Phys. Rev. B* **76**, 045302 (2007).
- [10] Y. L. Chen, J. G. Analytis, J.-H. Chu, Z. K. Liu, S.-K. Mo, X. L. Qi, H. J. Zhang, D. H. Lu, X. Dai, Z. Fang, S. C. Zhang, I. R. Fisher, Z. Hussain, and Z.-X. Shen, *Science* **325**, 178 (2009).
- [11] D. Hsieh, D. Qian, L. Wray, Y. Xia, Y. S. Hor, R. J. Cava, and M. Z. Hasan, *Nature (London)* **452**, 970 (2008).
- [12] T. Sato, K. Segawa, H. Guo, K. Sugawara, S. Souma, T. Takahashi, and Y. Ando, *Phys. Rev. Lett.* **105**, 136802 (2010).
- [13] Y. Xia, D. Qian, D. Hsieh, L. Wray, A. Pal, H. Lin, A. Bansil, D. Grauer, Y. S. Hor, R. J. Cava, and M. Z. Hasan, *Nat. Phys.* **5**, 398 (2009).
- [14] H. Zhang, C.-X. Liu, X.-L. Qi, X. Dai, Z. Fang, and S.-C. Zhang, *Nat. Phys.* **5**, 438 (2009).
- [15] M. Z. Hasan and C. L. Kane, *Rev. Mod. Phys.* **82**, 3045 (2010).
- [16] X.-L. Qi and S.-C. Zhang, *Rev. Mod. Phys.* **83**, 1057 (2011).
- [17] F. Wilczek, *Phys. Rev. Lett.* **58**, 1799 (1987).
- [18] J. Maciejko, X.-L. Qi, H. D. Drew, and S.-C. Zhang, *Phys. Rev. Lett.* **105**, 166803 (2010).
- [19] X.-L. Qi, T. L. Hughes, and S.-C. Zhang, *Phys. Rev. B* **78**, 195424 (2008).
- [20] L. Oroszlány and A. Cortijo, *Phys. Rev. B* **86**, 195427 (2012).
- [21] B. D. Tellegen, *Philips Res. Rep.* **3**, 81 (1948).
- [22] T. H. O’Dell, *Philos. Mag.* **7**, 1653 (1962).
- [23] L. D. Landau, J. S. Bell, M. Kearsley, L. Pitaevskii, E. Lifshitz, and J. Sykes, *Electrodynamics of Continuous Media*, Vol. 8 (Elsevier, Amsterdam, 2013).
- [24] L. Shaposhnikov, M. Mazanov, D. A. Bobylev, F. Wilczek, and M. A. Gorlach, *Phys. Rev. B* **108**, 115101 (2023).
- [25] M. M. Vazifeh and M. Franz, *Phys. Rev. Lett.* **111**, 027201 (2013).
- [26] A. Martín-Ruiz, M. Cambiaso, and L. F. Urrutia, *Phys. Rev. B* **99**, 155142 (2019).
- [27] E. Plum, J. Zhou, J. Dong, V. A. Fedotov, T. Koschny, C. M. Soukoulis, and N. I. Zheludev, *Phys. Rev. B* **79**, 035407 (2009).
- [28] I. Lindell, A. Sihvola, S. Tretyakov, and A. J. Viitanen, *Electromagnetic Waves in Chiral and Bi-isotropic Media* (Artech House, Boston, 1994).
- [29] A. N. Serdyukov, A. H. Sihvola, S. A. Tretyakov, and I. V. Semchenko, *Electromagnetics* **16**, 51 (1996).
- [30] A. Martín-Ruiz, M. Cambiaso, and L. F. Urrutia, *Phys. Rev. D* **92**, 125015 (2015).
- [31] A. Martín-Ruiz, M. Cambiaso, and L. F. Urrutia, *Phys. Rev. D* **93**, 045022 (2016).
- [32] A. Martín-Ruiz, *Phys. Rev. D* **98**, 056012 (2018).
- [33] A. Shuvaev, A. Pimenov, G. V. Astakhov, M. Mühlbauer, C. Brüne, H. Buhmann, and L. W. Molenkamp, *Appl. Phys. Lett.* **102**, 241902 (2013).
- [34] A. M. Shuvaev, G. V. Astakhov, G. Tkachov, C. Brüne, H. Buhmann, L. W. Molenkamp, and A. Pimenov, *Phys. Rev. B* **87**, 121104(R) (2013).
- [35] J. A. Crosse, S. Fuchs, and S. Y. Buhmann, *Phys. Rev. A* **92**, 063831 (2015).
- [36] J. A. Crosse, *Sci. Rep.* **7**, 43115 (2017).
- [37] L. Wu, M. Salehi, N. Koirala, J. Moon, S. Oh, and N. P. Armitage, *Science* **354**, 1124 (2016).
- [38] X.-L. Qi, R. Li, J. Zang, and S.-C. Zhang, *Science* **323**, 1184 (2009).
- [39] T. Melo, D. Viana, W. Moura-Melo, J. Fonseca, and A. Pereira, *Phys. Lett. A* **380**, 973 (2016).
- [40] W. Campos, W. Moura-Melo, and J. Fonseca, *Phys. Lett. A* **381**, 417 (2017).
- [41] L. Ge, T. Zhan, D. Han, X. Liu, and J. Zi, *Sci. Rep.* **5**, 7948 (2015).
- [42] K.-I. Imura, Y. Takane, and A. Tanaka, *J. Phys.: Conf. Ser.* **400**, 042021 (2012).
- [43] S. Ryu, J. E. Moore, and A. W. W. Ludwig, *Phys. Rev. B* **85**, 045104 (2012).
- [44] M. Tian, W. Ning, Z. Qu, H. Du, J. Wang, and Y. Zhang, *Sci. Rep.* **3**, 1212 (2013).
- [45] J. D. Jackson, *Classical Electrodynamics* (Wiley, Hoboken, NJ, 1998).
- [46] J. Ahn, S.-Y. Xu, and A. Vishwanath, *Nat. Commun.* **13**, 7615 (2022).
- [47] A. M. Shuvaev, G. V. Astakhov, A. Pimenov, C. Brüne, H. Buhmann, and L. W. Molenkamp, *Phys. Rev. Lett.* **106**, 107404 (2011).
- [48] A. Shuvaev, L. Pan, L. Tai, P. Zhang, K. L. Wang, and A. Pimenov, *Appl. Phys. Lett.* **121**, 193101 (2022).
- [49] J. A. Crosse, *Phys. Rev. A* **94**, 033816 (2016).
- [50] W.-K. Tse and A. H. MacDonald, *Phys. Rev. Lett.* **105**, 057401 (2010).
- [51] J. Yang, J. Kim, and K.-S. Kim, *Phys. Rev. B* **98**, 075203 (2018).
- [52] M. Ibanescu, Y. Fink, S. Fan, E. L. Thomas, and J. D. Joannopoulos, *Science* **289**, 415 (2000).
- [53] S. Nordebo, G. Cinar, S. Gustafsson, and B. Nilsson, *IEEE Trans. Microwave Theory Tech.* **63**, 1791 (2015).
- [54] P. B. Catrysse and S. Fan, *Phys. Rev. Lett.* **106**, 223902 (2011).
- [55] V. Shvedov and W. Krolikowski, *arXiv:1708.01998*.
- [56] Y. Zhou and M. N. Chen, *J. Phys.: Condens. Matter* **35**, 085001 (2023).
- [57] Since the surface charge and current densities σ_θ and \mathbf{K}_θ do satisfy a continuity equation, we will mostly refer to σ_θ . We note in passing that $\mathbf{K}_\theta \cdot \mathbf{E} = 0$, hence these induced charges and currents produce no Ohmic losses.
- [58] S. Filipini and M. Cambiaso (unpublished).
- [59] For elliptical polarization similar conclusions can be drawn. Subtle differences will be dealt with elsewhere [58].
- [60] The implications of Earnshaw’s theorem for the existence (or not) of TEM solutions are more “stringent” for cases with conductors. We defer this study in the context of θ -ED for Ref. [58].
- [61] A. G. Grushin and A. Cortijo, *Phys. Rev. Lett.* **106**, 020403 (2011).
- [62] O. J. Franca and S. Y. Buhmann, *Phys. Rev. B* **105**, 155120 (2022).
- [63] J.-P. Rivera, *Eur. Phys. J. B* **71**, 299 (2009).